ADVANCED FUNCTIONAL MATERIALS
www.afm-journal.de

FULL PAPER

A Versatile Light-Switchable Nanorod Memory: Wurtzite ZnO on Perovskite $SrTiO_3$

Ashok Bera, Haiyang Peng, James Lourembam, Youde Shen, Xiao Wei Sun, and T. Wu**

Integrating materials with distinct lattice symmetries and dimensions is an effective design strategy toward realizing novel devices with unprecedented functionalities, but many challenges remain in synthesis and device design. Here, a heterojunction memory made of wurtzite ZnO nanorods grown on perovskite Nb-doped $SrTiO_3$ (NSTO) is reported, the electronic properties of which can be drastically reconfigured by applying a voltage and light. Despite of the distinct lattice structures of ZnO and NSTO, a consistent nature of single crystallinity is achieved in the heterojunctions via the low-temperature solution-based hydrothermal growth. In addition to a high and persistent photoconductivity, the ZnO/NSTO heterojunction diode can be turned into a versatile light-switchable resistive switching memory with highly tunable ON and OFF states. The reversible modification of the effective interfacial energy barrier in the concurrent electronic and ionic processes most likely gives rise to the high susceptibility of the ZnO/NSTO heterojunction to external electric and optical stimuli. Furthermore, this facile synthesis route is promising to be generalized to other novel functional nanodevices integrating materials with diverse structures and properties.

1. Introduction

Synergistically integrating different functional materials on the nanometer-scale while maintaining tunability of properties over a wide range is the universal principle behind many modern electronic devices such as transistors, memories, and sensors. Transition metal oxides are ubiquitous in nature, and they exhibit a wide range of important physical properties and applications. Among notable ones, perovskite-structured complex oxides including $SrTiO_3$ (STO) are known for functionalities such as superconductivity,[1] colossal magnetoresistance,[2] ferroelectricity,[3] and thermoelectricity.[4] As another famous group of material, wurtzite-structured semiconductors like ZnO have been intensively pursued for optical, optoelectronic, sensing, magnetic, and energy harvesting applications.[5–10] Furthermore, both groups of materials have been recently investigated as active components in resistive switching resistive random access memories (RRAM) that show merits like low power consumption, high-speed operation, and high-density integration.[11–17] It is natural to envisage that the heterostructures synergistically combining perovskite and wurtzite oxides can provide unprecedented multifunctional devices that integrate the useful and unique properties of both material groups. However, as a result of their distinct crystalline structures, high-quality, low-cost and reliable growth of single-crystal perovskite-wurtzite heterostructures is rather challenging.

In this work, we focus on a particular perovskite-wurtzite heterostructure combining STO (cubic structure at room temperature with a = 3.905 Å) and ZnO (hexagonal structure with a = 3.249 Å and c = 5.206 Å). STO is the one of the most popular substrates for growing oxide thin films, and also a pioneer material of the emerging field of oxide electronics.[18–20] ZnO is a promising material for optoelectronic applications because of its wide band gap of 3.37 eV and large exciton binding energy of 60 meV.[21] It has also been used for other applications like piezoelectric generator[22,23] and biosensor.[24,25] Despite of the fact that STO and ZnO are two of the most intensively pursued oxides, there have been only a few reported attempts of growing ZnO on (001) STO substrates. In particular, pulsed laser deposition and metal-organic chemical vapour deposition were reported to lead to $(11\bar{2}0)$-oriented ZnO films with two orthogonal in-plane domain configurations.[26–30] There are even fewer reports dealing with the physical properties of ZnO/STO heterojunction. In one study, Wu et al. showed that ZnO thin films form nn^+ Schottky junctions with conducting Nb-doped STO (NSTO) substrates.[31] In another report, Zhang et al. studied the temperature dependence of resistive switching behaviour in ZnO/NSTO thin film heterojunctions.[32] However, so far there has been no report on the synthesis and properties of

Dr. A. Bera, H. Peng, J. Lourembam, Y. Shen, Prof. T. Wu
Division of Physics and Applied Physics
School of Physical and Mathematical Sciences
Nanyang Technological University
Singapore 637371, Singapore
E-mail: Tao.Wu@kaust.edu.sa
Prof. X. W. Sun
School of Electrical and Electronics Engineering
Nanyang Technological University
Singapore 639798, Singapore
E-mail: exwsun@ntu.edu.sg
Prof. X. W. Sun
South University of Science and Technology
1088 Xue-Yuan Road, Shenzhen, Guangdong 518055, China
Prof. T. Wu
Physical Sciences and Engineering Division
King Abdullah University of Science and Technology
Thuwal, 23955-6900, Saudi Arabia

DOI: 10.1002/adfm.201300509

© 2013 WILEY-VCH Verlag GmbH & Co. KGaA, Weinheim

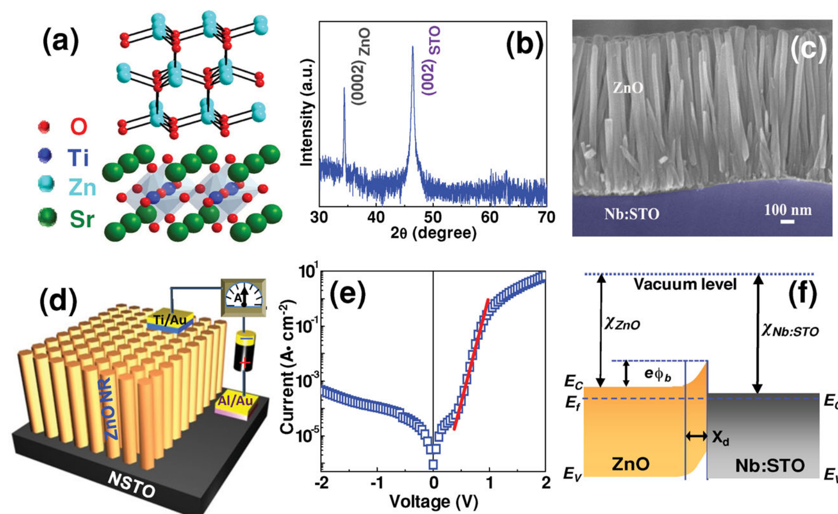

Figure 1. a) Atomic schematic representing wurtzite ZnO on perovskite $SrTiO_3$ with a shared c-axis orientation. b) XRD spectra in logrithmic scale and c) SEM image of the ZnO NRs grown on the conducting NSTO substrate. d) Schematic and measurement configuration of the ZnO NRs/NSTO heterojunction diode. e) Semi-log plot of the *J–V* characteristics of the ZnO/NSTO heterojunction. The linear line is a fit to the thermionic emission mechanism. f) Schematic of the equilibrium band alignment of the heterojunction at zero bias.

nanostructured heterojunction of ZnO on STO, which is the motivation behind our work. As the nanomaterials and their devices emerge as important building blocks in a myriad of electronic, photonic, biological, and energy applications, such diodes combining two prototypical oxides provide a pathway toward high-performance nanodevices.

Here, we report on the fabrication of single-crystal oxide diodes made of ZnO NRs grown via a low-temperature hydrothermal route on conducting NSTO (0.7 weight% Nb doping) substrates. In spite of the fact that diodes have a simple structure, they are the basis of diverse electronic devices such as integrated circuits, solar cells, optical devices, and light/gas sensors.[10,33–35] For the first time, we successfully synthesized and characterized such a single-crystal oxide diode made of two prototypical oxides with drastically different crystalline structures. At room temperature, ZnO NR/NSTO diodes show excellent characteristics with a rectification ratio of 6×10^3 at 2 V. On illumination of ultraviolet (UV) light, these heterojunction diodes exhibit a very high photo-to-dark current ratio (I_{ph}/I_d) of 1×10^4. Interestingly, they also show light-tunable resistive switching behaviors. Combining synergistically the functionalities of diode, photodetector and RRAM, these ZnO NR/NSTO single-crystal heterostructures are promising as integrated devices in advanced electronic and photonic applications.

2. Result and Discussion

2.1. Fabrication and Electrical Characterization of ZnO NRs/NSTO Single Crystal Diode

Figure 1a shows the schematic illustrating the wurtzite ZnO on top of the perovskite STO with a shared c-axis orientation. It is clear that epitaxial growth in the conventional high-temperature vapor phase method is difficult because of the distinct symmetries and the large lattice mismatch. Our strategy is to take advantage of the anisotropy growth speed in the solution-based hydrothermal synthesis to achieve c-axis aligned ZnO NRs on (001) STO substrates. The growth of such ZnO NRs is most likely driven by screw dislocations and this widely used facile method provides flexibility in controlling the morphology and properties of growth products.[36–38] In fact, this approach should be applicable to the growth of a wide range of nanomaterials on available supporting substrates as long as the substrates are stable in the solution environment at the growth temperature. As shown in Figure 1b, the X-ray diffraction spectrum of the sample shows both the ZnO (0002) peak at $2\theta = 34.2°$ and the NSTO (002) peak at $2\theta = 46.4°$, confirming that the ZnO NRs are single crystalline and grown along the c axis. The cross-sectional field emission scanning electron microscopy (FESEM) image in Figure 1c corroborates this result, showing that the NRs are vertically aligned on the NSTO substrates. Some of the NRs are broken as a result of the cleaving process during the sample preparation. The ZnO NRs have an average diameter of 43 ± 4 nm and a length of 1040 ± 10 nm. Their distribution is quite uniform with a density of about 440/μm^2.

Figure 1d shows the schematic of the electrical characterization of a ZnO NRs/NSTO heterojunction. In the transport measurements, Ti/Au and Al/Au electrodes form ohmic contacts with ZnO and NSTO, respectively, which was confirmed by the linear *I–V* characteristics of Au/Ti/ZnO/Ti/Au and Au/Al/NSTO/Al/Au junctions (Figure S1 in the Supporting Information). The room temperature *J–V* characteristics of ZnO NRs/NSTO heterojunction is plotted in semi-log scale in Figure 1e. We observed a diode-like behavior with very high rectification (ratio between forward and reverse currents, or I_F/I_R) of ≈6.1×10^3 at a bias of 2 V and ≈3.2×10^3 at 1 V. This rectification is higher than the previously reported values measured on similar heterojunctions, e.g., $I_F/I_R = 120$ for heterojunctions made of ZnO NWs and manganite thin films,[39] and $I_F/I_R = 40$ for ZnO NWs grown on polycrystalline manganite substrate.[40] The excellent rectification property observed here can be attributed to the suppressed current under the reverse bias which is on the order of 3.2×10^{-7}A at a bias of −2 V. This is a significant advantage compared to the junctions made of n-type ZnO NRs and p-type silicon where the rather large valence band offset makes the tunneling barrier very thin and leads to a high leakage current under the reverse bias.[41]

Although both ZnO and NSTO are n-type semiconductors, NSTO has a carrier concentration of the order of 10^{21} cm^{-3},[42] which is much higher than that of hydrothermally grown ZnO (≈10^{18} cm^{-3}).[5] Thus, ZnO NRs form nn$^+$ Schottky junctions with NSTO and it is expected that the depletion layer is mainly in the ZnO side (Figure 1f). We estimated the width of the depletion layer to be ≈13 nm according to $X_d = \sqrt{\frac{2\varepsilon_r |E_{fs} - E_{fm}|}{q^2 * N_d}}$, where

© 2013 WILEY-VCH Verlag GmbH & Co. KGaA, Weinheim

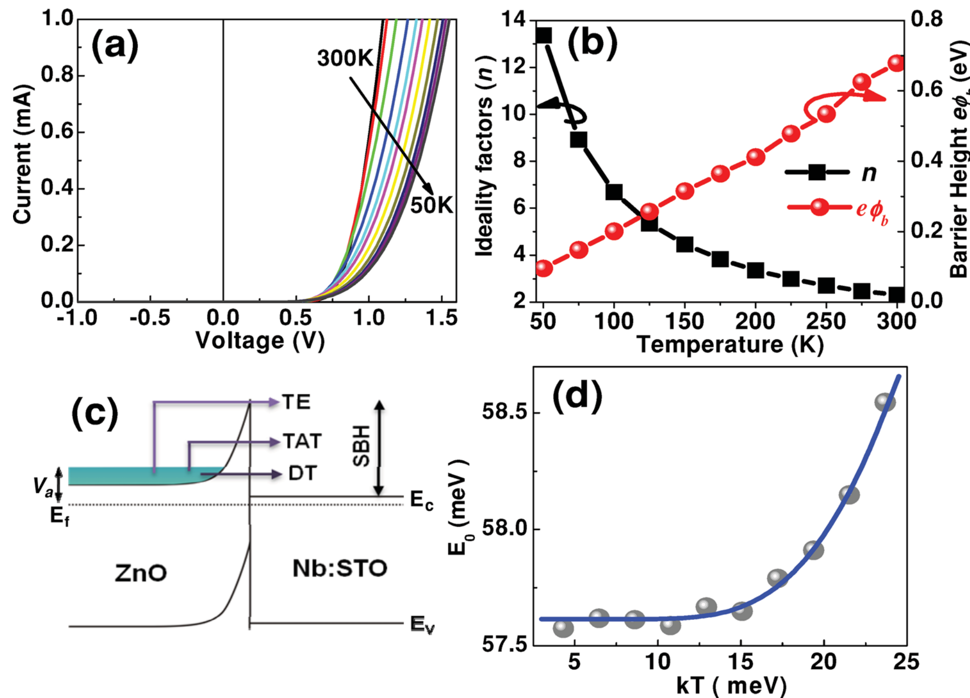

Figure 2. a) Temperature dependent *I–V* characteristics of the ZnO NRs/NSTO heterojunction diode. b) Temperature-dependent n and $e\varphi_b$ subtracted from fitting to the ideal thermoionic emission mechanism. c) Schematic potential profile for a ZnO NRs/NSTO Schottky junction along with different transport processes. TE, TAT and DT stand for thermionic emission, thermally assisted tunneling and direct tunneling, respectively. SBH is the Schottky barrier height, and V_a is the applied bias. d) Temperature dependence of the characteristic barrier E_0 derived by fitting to the TAT model.

ε_r is the dielectric constant of ZnO, N_d is the donor concentration of ZnO, q is the elemental charge, E_{fs} and E_{fm} are the Fermi energies for ZnO and NSTO, respectively. The work function of 0.7 wt% Nb doped STO is 4.2 eV,[43] and its Fermi level is very close to (0.016 eV below) the conduction band edge. The exact value of the electron affinity χ of ZnO depends on the details of the polar surface and the oxygen stoichiometry.[44] In determining the band alignment at the ZnO/STO interface, we used χ_{ZnO} = 3.8 eV with the Fermi level of ZnO lying 0.2 eV below the conduction band minimum.[44]

In general, current in a forward bias Schottky diode with a thermionic emission (TE) mechanism can be expressed as

$$I = I_0\left(\exp\frac{eV}{nkT} - 1\right) \tag{1}$$

where n is the diode ideality factor, e the electronic charge, k the Boltzmann constant, T the temperature, and I_0 is the reverse saturation current, which can be expressed as

$$I_0 = AA^*T^2\left(\exp\frac{e\phi_b}{kT}\right) \tag{2}$$

Here, A is the area of the diode, A^* is the Richardson constant (32 Acm^{-2} K^{-2} for ZnO), and φ_b is the Schottky barrier height. Using the above equation, we calculated n and φ_b from the linear region of the semi-log *J–V* curve (Figure 1e), and the calculated values are 2.3 and 0.67 eV, respectively. The ideality factor n is a measure of how closely the diode follows the ideal diode behavior. The ideality factor here is comparable to the value of 2.8 reported by Lao et al. for ZnO NR/Au Schottky diode.[45] There are two common reasons why n is higher than 1: One is the quantum mechanical tunneling of electrons through the interfacial barrier in the heterojunction, and the other is a high series resistance in the device. We calculated the series resistance of our device, and its value is very small (four orders smaller than the diode resistance at 0.7 volt, as given in Figure S2 in the Supporting Information). This suggests that the high value of n observed in our case is due to the tunneling current through the ZnO/NSTO interface.

2.2. Temperature-Dependent Thermionic Emission and Tunneling in the Diode Transport

To further investigate the presence of tunneling, we studied the *I–V* characteristics of the ZnO/NSTO heterojunction in a temperature range from 50 to 300 K (**Figure 2**a). The values of n and φ_b calculated as a function of temperature are given in Figure 2b. A significant increase of n was observed with decreasing temperature, indicating an enhanced role of electron tunneling in the diode current. Concomitantly, the calculated Schottky barrier height progressively shrinks to unphysical values at low temperatures (0.09 eV at 50 K), suggests notable deviation of the junction transport from the ideal Schottky behavior.

At very low temperatures, electron tunneling across the thin energy barrier can dictate the *I–V* characteristics of Schottky junctions,[46,47] and the energetic barrier at the junction interface depends on the deep-level trap states, which are generated

© 2013 WILEY-VCH Verlag GmbH & Co. KGaA, Weinheim

by lattice mismatch[48] and interfacial defects.[49] As a result of the distinct lattice structures of ZnO and STO, electrons traps with high densities are expected at the junction interfaces. With negligible thermal activation at very low temperatures, only direct tunneling (DT) is present in the junction transport, i.e., the electrons tunnel directly from the conduction band of the semiconductor to the metal (Figure 2c), and the voltage dependence of the forward bias current can be expressed as:

$$J^d = J_S^d \exp\left(\frac{eV}{E_{00}}\right) \tag{3}$$

and

$$E_{00} = \frac{eh}{4\pi}\left(\frac{N_{ZnO}}{m^{*}\varepsilon_{ZnO}}\right) \tag{4}$$

where h is the Plank constant, $\varepsilon_{\mathrm{ZnO}}$ is the permittivity of ZnO, and J_S^d can be considered as a constant with a weak dependence on temperature. In the intermediate temperature region, thermally assisted tunneling (TAT) occurs, where electrons are first excited to energy states higher than the Fermi level of the semiconductor and then tunnel to the metal side (Figure 2c). In this case, the forward bias current has the following voltage dependence:

$$J^{th} = J_S^{th} \exp\left(\frac{eV}{E_0}\right) \tag{5}$$

$$E_0 = E_{00} \coth\left(\frac{E_{00}}{kT}\right) \tag{6}$$

where E_{00} is the diffusion potential of the Schottky barrier.[50] From the I–V curves, we calculated the values of E_0 as a function of temperature (Figure 2d). When the temperature is low enough, E_0 is essentially temperature independent as expected for the case of DT, and a saturation value E_{00} = 57.6 meV is derived.

2.3. Persistent Photoconductivity in ZnO NRs/NSTO Single Crystal Diode

Figure 3a compares the I–V curves of the ZnO NRs/NSTO heterojunction measured both in dark and under illumination of UV light. As shown in the I–V curve 'B' with light, the reverse biased current is significantly enhanced in comparison to the pristine curve 'A" and as a result the curve is almost symmetric with respect to the voltage bias. This phenomenon is general in photodiodes where the photo-generated carriers dominate the transport;[51] under the reverse bias, electrons drift towards the positive electrode, whereas holes move to the negative electrode across the interface, leading to a high photocurrent. Furthermore, we observed persistent photo-current after turning off the UV light (curve 'C' in Figure 3a), and the complete recovery of the pristine state takes almost a day (curve 'D' in Figure 3a).

We also measured the transient photocurrents of the junctions by periodically turning on and off the UV light (Figure 3b). The growth-and-decay spectra of photocurrent show that on UV illumination the currents of both the ZnO NRs and the ZnO NRs/NSTO junctions quickly increase to very high values, leading to photo-to-dark current ratios of 5 × 10^3 and 1 × 10^4, respectively. On the other hand, as a result of the high dark current, the NSTO single crystal shows only a small increase in

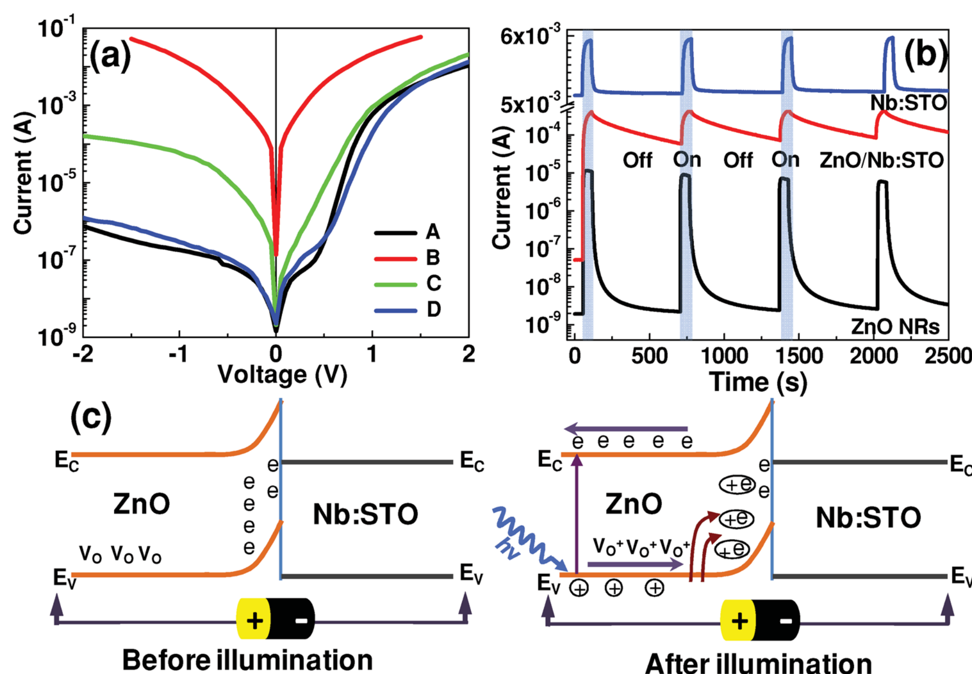

Figure 3. a) I–V characteristics of the ZnO NRs/NSTO heterojunction measured under various conditions of UV illumination. Curve 'A': the pristine one before UV illumination; 'B': under the presence of UV light; 'C': one hour after turning off the light; 'D': one day after turning off the light. b) Transient photoresponse of ZnO NRs, NSTO and ZnO NRs/NSTO heterojunctions measured under periodic light illumination and a voltage bias of –0.2 V. c) Schematic illustration of charge separation and persistent photocurrent in the reverse-biased heterojunction under the illumination of UV light.

© 2013 WILEY-VCH Verlag GmbH & Co. KGaA, Weinheim

current under the light illumination. When the light is turned off, for both ZnO NRs and NSTO, the current decays almost instantly to its dark value, but in the case of ZnO NRs/NSTO, persistent photocurrent (PPC) was observed. Although the diode current still exhibits response to the switching of UV light, it does not come back to the pristine dark value when the light is off. PPC has been previously reported in semiconductor heterostructures such as thin GaAs layers and $LaAlO_3/SrTiO_3$ interfaces where macroscopic potential barriers at junctions spatially separate the photogenerated electron/hole pairs.[52,53] This effect is relevant to applications in bistable optical switches and radiation detectors.[54,55] One potential explanation of PPC is the light-induced desorption of surface oxygen species in the photoconduction and their subsequent re-absorption, causing the slow decay of current in the dark.[56] But this mechanism can be ruled out here because the PPC persists even under vacuum. Instead, the mechanism of PPC is likely related to both the photogenerated carriers and the ionized defects which migrate to the junction region under the influence of electrical field. As shown in Figure 3c, under the illumination of UV light, the photogenerated electrons move towards the anode, whereas holes move towards the interface to recombine with the electrons trapped in the space charge region. In addition, some trapped electrons in oxygen vacancies can also be photo-excited to the conduction band and the ionized oxygen vacancies will move toward the interface due to the presence of macroscopic potential barrier at the ZnO/NSTO interface.[57] The captured holes and the ionized oxygen vacancies have long lifetimes because of their large effective mass and low mobility, and their slow drifting back to the original states leads to the occurrence of PPC.

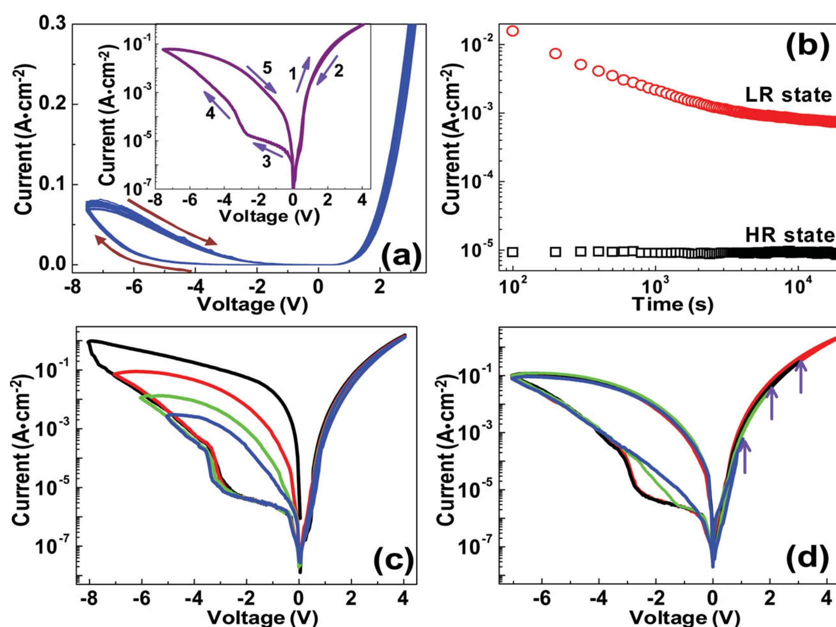

Figure 4. a) *I–V* switching loop for 30 cycles. For clarity, the absolute value of the reverse current is plotted. Inset is the semi-log plot for a single loop with the scanning sequence and directions marked. b) Retention data of the ZnO NRs/NSTO heterojunction. Both ON and OFF states were measured at –2 V. c) Switching loops showing the modulation of the LR state via scanning to different maximum negative voltages. d) Switching loops showing the modulation of the HR state as a result of different maximum positive voltages. The arrows mark the maximum positive voltages for different loops.

2.4. Tunable Nonvolatile Resistive Switching Behavior

So far in the discussion of transport measurements of ZnO NR/STO single crystal diodes, we have limited the range of voltage bias within –2 and +2 V, and the measured *I–V* curves show negligible hysteresis. Interestingly, when we expanded the range of measurement voltage, the ZnO NRs/NSTO junctions exhibited memristive behaviors in transport. **Figure 4**a shows the typical resistive switching behavior of the heterojunction, and the overlap of thirty successively measured *I-V* loops reflects the device endurance. The inset of Figure 4a presents a typical *I–V* loop in the semi-log scale, which reveals a quite unique switching behavior: no hysteresis in the forward bias region (scan steps 1 and 2), whereas an electrical bi-stability appears at the reverse bias (steps 3 to 5). For the conventional resistive switching devices, a forming process is essential, which prepares the devices into the switchable state. As shown in the inset, at low reverse bias, the device stays at the high resistance (HR) or the "OFF" state. But when the applied bias crosses –3 V a drastic increase of current appears (transition from step 3 to step 4) and this set process switches the device into the low resistance (LR) or the "ON" state. The ON/OFF ratio is more that 10^3 at an applied voltage of –2 V.

The observed switching behavior of the heterojunction diode can be explained by the reversible migration of charged defects, in particular ionized oxygen vacancies, in the vicinity of the ZnO/NSTO interface. The important role of the dynamics of such ionized defects under the electrical and thermal stimuli has been well recognized in resistive switching heterojunction devices.[58–61] Particualrly, ZnO often contains high-density oxygen vacancies which have a very low formation energy and remain positively ionized.[62,63] When the junction is reversely biased, i.e., a positive bias on ZnO and a negative bias on NSTO, oxygen vacancies in ZnO are dragged into the interface region. These oxygen vacancies are trapped at the interface and effectively reduce the energy barrier. When the interfacial barrier becomes thin enough at a sufficiently high reverse voltage, electrons tunnel from the NSTO side to the ZnO side, setting the device into the LR state. This process is reversed when the device is forward biased and the negative voltage applied to the ZnO end pulls the oxygen vacancies away from the interface, recovering the depletion layer and resetting the device back to the HR state. As a confirmation to the proposed mechanism, the voltage dependence of the current in the LR state indeed follows the equation $J \approx A\sinh(BV)$ with A and B being junction-specific constants, which is typical for the electron tunneling process[11] (Figure S3, Supporting Information).

The retention data in Figure 4b show that the ON/OFF ratio of the device remains more than 10^2 after 2×10^4 s. The slow decay of the LR state could be related to the diffusion of oxygen vacancies away from the interface

© 2013 WILEY-VCH Verlag GmbH & Co. KGaA, Weinheim

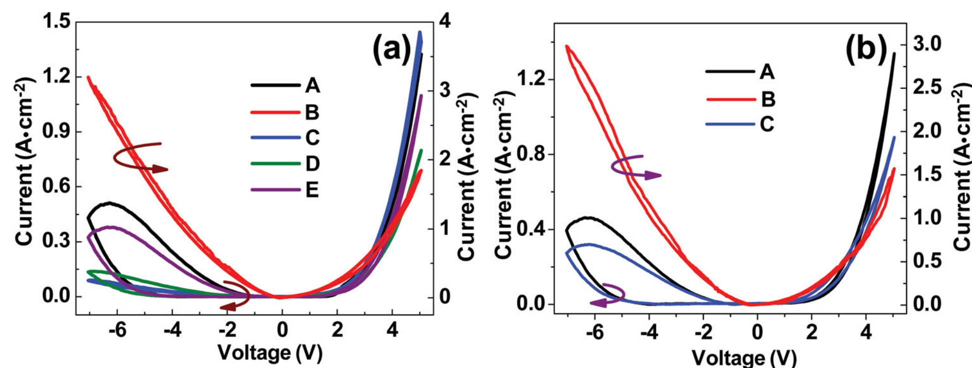

Figure 5. a) Resistive switching behaviors under various conditions, i.e., 'A': Before illumination; 'B': During illumination; 'C': 30 min after turning off the light; 'D': One hour after turning off the light; E: One day after turning off the light. b) Effect of annealing on the resistive switching of our device. 'A': The pristine state before UV illumination; 'B': During UV illumination; 'C': the resistive switching behavior was recovered after annealing at 300 °C for 5 min.

region, and the LR resistance approaches the equilibrium value during the retention test. The endurance data can be found in Figure S4, Supporting Information. Furthermore, Figures 4c,d show that the ON and OFF current values can be tuned by simply adjusting the applied maximum voltages. In Figure 4c, we fixed the maximum positive voltage to 4 V, which keeps the HR state unchanged. As the maximum negative voltage is adjusted form −5 to −8 V, the HR current density increases significantly and the ON/OFF ratio at −2 V improves from 10^2 to 10^4. Nagashima et al. also reported that by changing the maximum complience current from 10^{-10} to 10^{-8} A the ON/OFF ratio can improve from 3 to 300 in memory devices based on individual cobalt oxide nanowires.[64] The observed tunability of the LR state in our experiments is consistent with the scenario of migrating oxygen vacancies because a higher negative voltage will move more oxygen vacancies to the depletion layer and make the energy barrier thinner, causing more electron tunneling events and a higher LR current. We also measured the switching loops by keeping the maximum negative voltage at −7 V while increasing the maximum positive voltage from 1 V to 4.5 V. It is clear from Figure 4d that the shape of the hysteresis loops in the negative voltage regime strongly depends on the value of the maximum positive voltage; when the applied maximum positive voltage is less than 3 V, the device cannot be switched completely to the HR state. This again can be explained by the proposed ionic mechanism because the recovery of the energy barrier requires a sufficiently high voltage to move the ionized oxygen vacancies out of the interfacial depletion region. The observed flexibility in tuning the ON and OFF states in Figure 4c,d is important for the application of such ZnO NRs/NSTO single crystal diodes in multi-level resistive switching memory devices with improved scalability and integration capability.

2.5. Light-Tunable Resistive Switching in ZnO NRs/NSTO Single Crystal Diodes

Interestingly, we found that the UV light can cause significant modulation of the resistive switching behavior of our devices. **Figure 5**a shows the resistive switching loops collected under various conditions of UV illumination. Since the reverse bias current under UV illumination is very high and mainly dominated by the photo-excited carriers, the ZnO NRs/NSTO heterojunction diode show negligible switching in the presence of UV light. Even 30 min after the UV light was turned off, no obvious hysteresis and switching was observed. But one hour after turning off the UV light, some switching was observed although the hysteresis loop remains rather narrow. The pristine resistive switching behavior was fully recovered only after the device was kept in dark for one day, and this result is comparable to the one observed in the persistent photoconductivity measurements.

For applications combining the functionalities of photodiode and memristor, it is essential that the pristine state of our devices can be recovered as fast as possible. However, the data in Figure 5a clearly indicates that the UV light creates a persistent effect on the switching capability of our devices. Here it is important to note that the persistent behavior in transport after the UV illumination originates from the charge and defect trapping at the ZnO/NSTO interface, which separates the photo-generated electrons from their parent donors. Thus, we hypothesize that a brief thermal annealing process can provide the activation energy for the release of the positively trapped charges and defects at the interface, leading to the fast recovery of the pristine state. Indeed, we found that annealing our device at 300 °C for only 5 min after the UV illumination is sufficient to recover the pristine switchable state (Figure 5b). To fully exploit the functionality of the ZnO NRs/NSTO heterojunctions we performed consecutive write/read/erase/read experiments with a series of different set and reset voltages. We first applied voltage pulses with a duration of five milliseconds in the sequence of −7.5V/4V/−5V/4V/−7.5V/1V in the dark condition (regime I), and the states of the diode were read between the pulses. As shown in **Figure 6**, data can be reliably written, read, and erased; furthermore, the values of ON state current and OFF state current can be modulated to a large degree by adjusting the magnitude of the applied voltage pulses. In contrast, under the illumination of UV light (regime II), the HR state and LR state exhibit almost the same high values of current and the device is effectively deactivated. Finally, the switching capability of the heterojunction can be

© 2013 WILEY-VCH Verlag GmbH & Co. KGaA, Weinheim

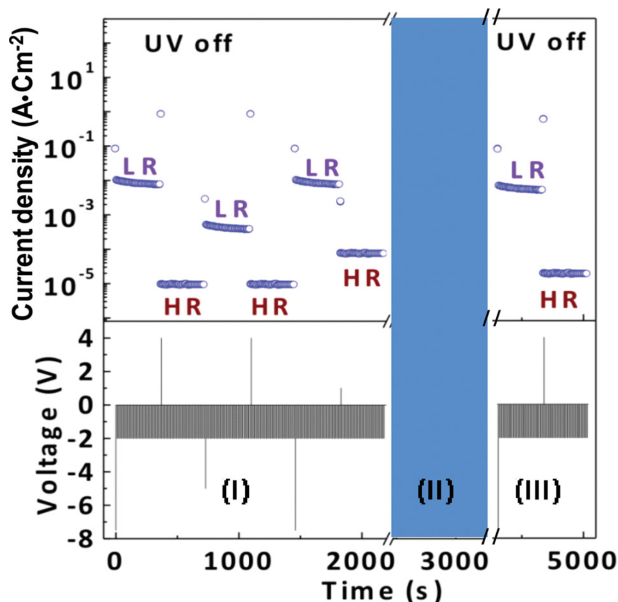

Figure 6. Multiple resistance states (upper panel) achieved under various electrostatic and illumination conditions (lower panel). The switched states were read with a voltage of –2 V, and the device exhibits a data retention capability throughout the process. Three representative regimes are shown: (I) before illumination, (II) during illumination (III) after annealing treatment.

fully recovered after the annealing treatment at 300 °C for five minutes (regime III). As indicated by the switching behaviors shown in region (III) the device clearly recovered its pristine switching states after annealing. It is interesting to note that our result is different from the recently reported light-induced resistive switching in a metal-insulator-semiconductor heterostructure[65] or a metal-semiconductor-metal heterostructure[66] where the switching was observed only in the presence of light. This comparison clearly underscores the strong structure-property correlation in such resistive switching heterojunctions.

3. Conclusion

We synthesized for the first time a heterojunction RRAM composed of two prototypical oxides: ZnO NRs on $SrTiO_3$ substrate, which have shared single crystallinity formed via the facile aqueous chemical growth route. The Schottky diode presents excellent rectification properties with a high forward-to-reverse bias ratio of 10^3, which is accompanied with a photo detection capability and a photo-to-dark current ratio of 10^4. Furthermore, our device exhibits resistive switching and data retention behaviors which are featured with bias-tuned multilevel data storage. The voltage and photo sensitive functionalities of the ZnO/STO heterojunction diodes hinge on the reversible reconfiguration of ionic defects near the interface region, which in turn modifies the electronic tunneling and emission across the Schottky barrier. In a broad perspective, our results provide a general and facile route toward integrating functional materials with distinct crystalline structures into heterojunction devices which can serve as nanoscale memories, switches and sensors operating in complementary electrical and optical modes.

4. Experimental Section

Synthesis: The vertically aligned ZnO NRs were grown on the NSTO substrates using aqueous citrate-assisted hydrothermal growth method as described in previous reports.[60] In brief, 0.1 M solutions of zinc acetate dehydrate [$(CH_3COO)_2Zn{\cdot}2H_2O$] (Sigma-Aldrich) were prepared in propanol solvent using diethanolamine as a stabilizer. The solution was spin coated on the cleaned NSTO substrates at a speed of 2500 rpm. Then the substrates were dried at 120 °C for 20 min and annealed at 400 °C for 30 min. To grow ZnO NRs, the seeded NSTO substrates were dipped into an equimolar (0.015 M) solution of $(CH_3COO)_2Zn{\cdot}2H_2O$ and hexamethylenetetramine $(CH_2)_6N_4$ in de-ionized water which was prepared by vigorous stirring for 1 h. A typical growth occurs at 90 °C for one hour. Finally the substrates were removed from the solution, rinsed in de-ionized water and dried.

Characterization: The structure and the morphology of the ZnO NRs were examined by X-ray diffractometer (Bruker D8) and field emission scanning electron microscopy (FESEM, JEOL JSM-6700F). For the electrical characterizations, Ti/Au (10/50 nm) and Al/Au (20/50 nm) electrodes with dimensions of 200 μm × 200 μm were deposited by sputtering on the ZnO NRs and the NSTO substrate, respectively. The current-voltage data were measured using a source meter (Keithley2635). The photoresponse of the ZnO/NSTO diode was measured by illuminating the samples with monochromatic light of wavelength 365 nm and intensity 2.5 W/cm^2 from a solid state UV LED (Agiltron 365A). During the photoresponse measurements, the diode was reverse biased with a voltage of –0.2 V.

Supporting Information

Supporting Information is available from the Wiley Online Library or from the author.

Acknowledgements

This work is partially supported by the National Research Foundation of Singapore through the Competitive Research Programme (CRP Award No. NRF-CRP-4-2008-04), the Science and Engineering Research Council, Agency for Science, Technology and Research (A*STAR) of Singapore (project No. 092 151 0088), and the National Natural Science Foundation of China (NSFC) (project Nos. 61006037 and 61076015).

Received: February 7, 2013
Revised: March 9, 2013
Published online: April 25, 2013

[1] K. Ueno, S. Nakamura, H. Shimotani, A. Ohtomo, N. Kimura, T. Nojima, H. Aoki, Y. Iwasa, M. Kawasaki, *Nat. Mater.* **2008**, *7*, 855.
[2] S. Jin, T. H. Tiefel, M. McCormack, R. A. Fastnacht, R. Ramesh, L. H. Chen, *Science* **1994**, *264*, 413.
[3] M. Dawber, K. M. Rabe, J. F. Scott, *Rev. Mod. Phys.* **2005**, *77*, 1083.
[4] H. Ohta, S. Kim, Y. Mune, T. Mizoguchi, K. Nomura, S. Ohta, T. Nomura, Y. Nakanishi, Y. Ikuhara, M. Hirano, H. Hosono, K. Koumoto, *Nat. Mater.* **2007**, *6*, 129.
[5] M. Law, L. E. Greene, J. C. Johnson, R. Saykally, P. Yang, *Nat. Mater.* **2005**, *4*, 455.
[6] R. X. Yan, D. Gargas, P. D. Yang, *Nat. Photonics* **2009**, *3*, 569.
[7] Z. L. Wang, J. H. Song, *Science* **2006**, *312*, 242.

© 2013 WILEY-VCH Verlag GmbH & Co. KGaA, Weinheim

[8] Y. B. Zhang, Q. Liu, T. Sritharan, C. L. Gan, S. Li, *Appl. Phys. Lett.* **2006**, *89*, 042510.
[9] G. Z. Shen, Y. Bando, B. D. Liu, D. Golberg, C. J. Lee, *Adv. Funct. Mater.* **2006**, *16*, 410.
[10] G. Shen, P. C. Chen, K. Ryu, C. Zhou, *J. Mater. Chem.* **2009**, *19*, 828.
[11] J. J. Yang, M. D. Pickett, X. Li, D. A. Ohlberg, D. R. Stewart, R. S. Williams, *Nat. Nanotechnol.* **2008**, *3*, 429.
[12] A. B. K. Chen, B. J. Choi, X. Yang, I. W. Chen, *Adv. Funct. Mater.* **2012**, *22*, 546.
[13] J. Qi, M. Olmedo, J. J. Ren, N. Zhan, J. Z. Zhao, J. G. Zheng, J. L. Liu, *ACS Nano* **2012**, *6*, 1051.
[14] D. Pantel, S. Goetze, D. Hesse, M. Alexe, *ACS Nano* **2011**, *5*, 6032.
[15] A. Ruotolo, C. W. Leung, C. Y. Lam, W. F. Cheng, K. H. Wong, G. P. Pepe, *Phys. Rev. B* **2008**, *77*, 233103.
[16] W. Jiang, M. Noman, Y. M. Lu, J. A. Bain, P. A. Salvador, M. Skowronski, *J. Appl. Phys.* **2011**, *110*, 034509.
[17] S. Menzel, M. Waters, A. Marchewka, U. Bottger, R. Dittmann, R. Waser, *Adv. Funct. Mater.* **2011**, *21*, 4487.
[18] M. Kawasaki, K. Takahashi, T. Maeda, R. Tsuchiya, M. Shinohara, O. Ishiyama, T. Yonezawa, M. Yoshimoto, H. Koinuma, *Science* **1994**, *266*, 1540.
[19] A. Ohtomo, H. Y. Hwang, *Nature* **2004**, *427*, 423.
[20] J. Mannhart, D. G. Schlom, *Science* **2010**, *327*, 1607.
[21] M. H. Huang, S. Mao, H. Feick, H. Q. Yan, Y. Y. Wu, H. Kind, E. Weber, R. Russo, P. D. Yang, *Science* **2001**, *292*, 1897.
[22] X. D. Wang, J. H. Song, J. Liu, Z. L. Wang, *Science* **2007**, *316*, 102–105.
[23] Z. L. Wang, *Adv. Funct. Mater.* **2008**, *18*, 3553.
[24] S. Saha, V. Gupta, K. Sreenivas, H. H. Tan, C. Jagadish, *Appl. Phys. Lett.* **2010**, *97*, 133704.
[25] P. H. Yeh, Z. Li, Z. L. Wang, *Adv. Mater.* **2009**, *21*, 4975.
[26] C. H. Jia, Y. H. Chen, G. H. Liu, X. L. Liu, S. Y. Yang, Z. G. Wang, *J. Phys. D: Appl. Phys.* **2009**, *42*, 015415.
[27] M. Karger, M. Schilling, *Phys. Rev. B* **2005**, *71*, 075304.
[28] Y. Wu, L. Zhang, G. Xie, J. Ni, Y. Chen, *Solid State Commun.* **2008**, *148*, 247.
[29] E. Bellingeri, D. Marre, I. Pallecchi, L. Pellegrino, A. S. Siri, *Appl. Phys. Lett.* **2005**, *86*, 012109.
[30] X. H. Wei, Y. R. Li, J. Zhu, W. Huang, Y. Zhang, W. B. Luo, H. Ji, *Appl. Phys. Lett.* **2007**, *90*, 151918.
[31] Y. Wu, L. Zhang, G. Xie, J. L. Zhu, Y. Chen, *Appl. Phys. Lett.* **2008**, *92*, 012115.
[32] H. J. Zhang, X. P. Zhang, Y. G. Zhao, *Chin. Phys. Lett.* **2009**, *26*, 077303.
[33] A. Ruotolo, C. Y. Lam, W. F. Cheng, K. H. Wong, C. W. Leung, *Phys. Rev. B* **2007**, *76*, 075122.
[34] P. C. Chen, G. Z. Shen, H. T. Chen, Y. G. Ha, C. Wu, S. Sukcharoenchoke, Y. Fu, J. Liu, A. Facchetti, T. J. Marks, M. E. Thompson, C. W. Zhou, *ACS Nano* **2009**, *3*, 3383.
[35] R. Lecover, N. Williams, N. Markovic, D. H. Reich, D. Q. Naiman, H. E. Katz, *ACS Nano* **2012**, *6*, 2865.
[36] L. Vayssieres, K. Keis, S. E. Lindquist, A. Hagfeldt, *J. Phys. Chem. B* **2001**, *105*, 3350.
[37] K. Govender, D. S. Boyle, P. B. Kenway, P. O'Brien, *J. Mater. Chem.* **2004**, *14*, 2575.
[38] S. A. Morin, A. Forticaux, M. J. Bierman, S. Jin, *Nano Lett.* **2011**, *11*, 4449.
[39] Z. Zhang, Y. Sun, Y. Zhao, G. Li, T. Wu, *Appl. Phys. Lett.* **2008**, *92*, 103113.
[40] S. Mridha, D. Basak, *Nanotechnology* **2009**, *20*, 075203.
[41] H. Sun, Q. F. Zhang, J. L. Wu, *Nanotechnology* **2006**, *17*, 2271.
[42] T. Tomio, H. Miki, H. Tabata, T. Kawai, S. Kawai, *J. Appl. Phys.* **1994**, *76*, 5886.
[43] G. Li, T. F. Zhou, D. D. Hu, Y. P. Yao, Y. Hou, X. G. Li, *Appl. Phys. Lett.* **2007**, *91*, 163114.
[44] K. Jacobi, G. Zwicker, A. Gutmann, *Surf. Sci.* **1984**, *141*, 109.
[45] C. S. Lao, J. Liu, P. Gao, L. Zhang, D. Davidovic, R. Tummala, Z. L. Wang, *Nano Lett.* **2006**, *6*, 263.
[46] F. A. Padovani, R. Stratton, *Solid-State Electron.* **1966**, *9*, 695.
[47] C. Y. Chang, S. M. Sze, *Solid-State Electron.* **1970**, *13*, 727.
[48] C. D. Bessire, M. T. Bjork, H. Schmid, A. Schenk, K. B. Reuter, H. Riel, *Nano Lett.* **2011**, *11*, 4195.
[49] A. M. Cowley, S. M. Sze, *J. Appl. Phys.* **1965**, *36*, 3212.
[50] Y. W. Yin, J. F. Ding, J. Wang, L. Xie, Q. X. Yu, X. G. Li, *J. Appl. Phys.* **2010**, *107*, 053915.
[51] S. Mridha, D. Basak, *J. Appl. Phys.* **2007**, *101*, 083102.
[52] A. Tebano, E. Fabbri, D. Pergolesi, G. Balestrino, E. Traversa, *ACS Nano* **2012**, *6*, 1278.
[53] H. J. Queisser, D. E. Theodorou, *Phys. Rev. Lett.* **1979**, *43*, 401.
[54] R. C. Jayasinghe, G. Ariyawansa, N. Dietz, A. G. U. Perera, S. G. Matsik, H. B. Yu, I. T. Ferguson, A. Bezinger, S. R. Laframboise, M. Buchanan, H. C. Liu, *Opt. Lett.* **2008**, *33*, 2422.
[55] T. Tanabe, M. Notomi, S. Mitsugi, A. Shinya, E. Kuramochi, *Opt. Lett.* **2005**, *30*, 2575.
[56] Y. Z. Jin, J. P. Wang, B. Q. Sun, J. C. Blakesley, N. C. Greenham, *Nano Lett.* **2008**, *8*, 1649.
[57] S. Lany, A. Zunger, *Phys. Rev. B* **2005**, *72*, 035215.
[58] K. Nagashima, T. Yanagida, K. Oka, M. Kanai, A. Klamchuen, J. S. Kim, B. H. Park, T. Kawai, *Nano Lett.* **2011**, *11*, 2114.
[59] K. Nagashima, T. Yanagida, K. Oka, M. Kanai, A. Klamchuen, S. Rahong, G. Meng, M. Horprathum, B. Xu, F. Zhuge, Y. He, B. H. Park, T. Kawai, *Nano Lett.* **2012**, *21*, 5684.
[60] J. J. Yang, D. B. Strukov, D. R. Stewart, *Nat. Nanotechnol.* **2013**, *8*, 13.
[61] D. B. Strukov, R. S. Williams, *Appl. Phys. A* **2009**, *94*, 515.
[62] P. D. Yang, H. Q. Yan, S. Mao, R. Russo, J. Johnson, R. Saykally, N. Morris, J. Pham, R. R. He, H. J. Choi, *Adv. Funct. Mater.* **2002**, *12*, 323.
[63] X. Wang, Q. Q. Li, Z. B. Liu, J. Zhang, Z. F. Liu, R. M. Wang, *Appl. Phys. Lett.* **2004**, *84*, 4941.
[64] K. Nagashima, T. Yanagida, K. Oka, M. Taniguchi, T. Kawai, J. S. Kim, B. H. Park, *Nano Lett.* **2010**, *10*, 1359.
[65] M. Ungureanu, R. Zazpe, F. Golmar, P. Stoliar, R. Llopis, F. Casanova, L. E. Hueso, *Adv. Mater.* **2012**, *24*, 2496.
[66] J. Park, S. Lee, K. Yong, *Nanotechnology* **2012**, *23*, 385707.
[67] A. Bera, D. Basak, *Appl. Phys. Lett.* **2008**, *93*, 053102.

© 2013 WILEY-VCH Verlag GmbH & Co. KGaA, Weinheim